

Rolling and Sliding Modes of Nanodroplet Spreading: Molecular Simulations and a Continuum Approach

Sreehari Perumanath^{1,*}, Mykyta V. Chubynsky^{1,2,†}, Rohit Pillai^{3,‡}, Matthew K. Borg^{1,3,§} and James E. Sprittles^{1,||}

¹Mathematics Institute, University of Warwick, Coventry CV4 7AL, United Kingdom

²Centre for Fluid and Complex Systems, Coventry University, Coventry, CV1 5FB, United Kingdom

³School of Engineering, University of Edinburgh, Edinburgh EH9 3FB, United Kingdom

 (Received 12 September 2022; revised 11 May 2023; accepted 15 August 2023; published 19 October 2023)

Molecular simulations discover a new mode of dynamic wetting that manifests itself in the very earliest stages of spreading, after a droplet contacts a solid. The observed mode is a “rolling” type of motion, characterized by a contact angle lower than the classically assumed value of 180° , and precedes the conventional “sliding” mode of spreading. This motivates the development of a novel continuum framework that captures all modes of motion, allows the dominant physical mechanisms to be understood, and permits the study of larger droplets.

DOI: 10.1103/PhysRevLett.131.164001

Dynamic wetting governs a wealth of physical systems ranging from surface coatings [1,2] to the guided folding of graphene flakes [3]. In recent decades, a drive toward miniaturization of fluid-based technologies has created a surge of interest in wetting, initially, at the microscale and, more recently, at the nanoscale, e.g., for nanoprinting [4] or 3D printed bionic nanodevices [5]. Fluid behavior at these scales can be nonintuitive and occur in a regime where experiments are rare, molecular dynamics (MD) simulations can be tractable, and the validity of conventional theoretical approaches is questionable [6–8].

Motivated by practical applications, much research has focused on how droplets can be deposited onto solid surfaces. In particular, the impact phase involving the displacement of an ambient air cushion has attracted great interest due to surprising experimental observations [9,10]. In contrast, the initial stages of spreading postcontact have received far less attention, despite their importance for understanding spontaneous capillary-driven wetting, rapid adhesion produced by insects [11], or bioinspired switchable capillary-based grips [12].

The initial radial spreading of millimeter-sized droplets on solids has been probed using high-speed cameras [13–16]. However, side-on imaging cannot visualize the cusplike geometry created at the early stages, which means that the liquid-solid-gas contact line (CL) of a millimeter-sized droplet cannot be observed until it has wet a radius of $r_{CL} \sim 100 \mu\text{m}$ [13]. Viewing from under the substrate significantly improves matters [14], but measurements are possible only

once $r_{CL} \sim 10 \mu\text{m}$. At these microfluidic scales (and above), conventional theories of wetting are valid and lead to known scaling laws. However, experimental investigations have yet to probe the very earliest stages of contact and spreading, where there is significant debate surrounding the validity of conventional approaches [6,17].

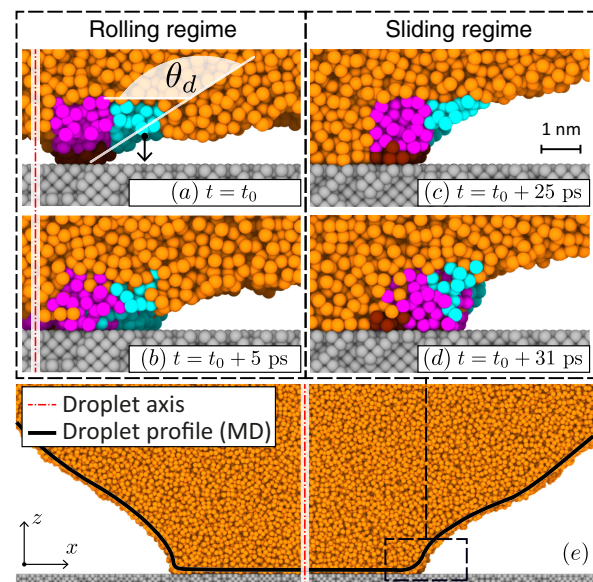


FIG. 1. MD close-up snapshots near the CL of a quasi-2D water droplet ($R = 29.8 \text{ nm}$, $\theta_e \approx 63^\circ$). (a),(b) Immediately after contact, the CL evolves in a rolling regime, where the (cyan) interfacial molecules traverse the narrow gap to meet the solid. Here, $\theta_d < 180^\circ$. (c),(d) Later, the CL advances via a sliding regime, where the contribution from interfacial molecules in driving the CL is minimal. Note that the molecules are recolored in (c). (e) The extracted droplet profile on top of the corresponding MD snapshot.

Published by the American Physical Society under the terms of the Creative Commons Attribution 4.0 International license. Further distribution of this work must maintain attribution to the author(s) and the published article's title, journal citation, and DOI.

From a theoretical perspective, when viscous and capillary forces are negligible compared to inertial ones, rolling motion can be observed in drop impact [18]. However, in regimes where they are not, the classical fluid dynamics framework is known to fail for dynamic wetting [19–22], and solutions are usually sought by assuming either (a) slip between the liquid and solid [23–25] or (b) perfect rolling of the CL, with the dynamic contact angle θ_d fixed at 180° [26–29].

In conventional slip flows, sliding-type dynamics are usually described by a molecular kinetic theory [30,31] and/or a Cox-Voinov framework [32,33]; see [34] for details. In contrast, rolling-type motion with fixed $\theta_d = 180^\circ$ can be consistently used with a no-slip condition: It has been studied theoretically by various groups [26–28]. While such analyses are useful for approximating motion on highly nonwetable surfaces or for exotic systems, such as Leidenfrost droplets [29] or liquid marbles [35], this mode of motion has not been observed for drops spreading spontaneously on partially wetting solids.

In this Letter, MD will lead to the discovery of a new class of rolling-type CL motion, which is crucial for—and dominant in—the very earliest stages of wetting, with $\theta_d < 180^\circ$ [see Figs. 1(a) and 1(b)]. This new regime of wetting bridges the first contact with the conventional sliding regime of CL motion [see Figs. 1(c) and 1(d)]. The key physics governing this regime is shown to be the long-range interaction forces between liquid and solid molecules, and, by incorporating this physics into a novel computational model, we can efficiently reproduce computationally expensive MD data, identify governing physical parameters, and investigate systems at larger scales. In doing so, new research challenges will be identified and discussed.

MD simulation details.—MD [36] has a long history of being used as a virtual experiment for small-scale fluid dynamics, e.g., [37–39]. To permit the simulation of relatively large water droplets, we use the “mW model” [40] and primarily investigate the spreading of quasi-2D cylindrical droplets in pure vapor on a solid that has an fcc lattice structure. Solid molecules interact with those in the liquid via the Lennard-Jones (LJ) potential

$$U_{jk} = 4\epsilon_{SL} \left[\left(\frac{\sigma}{r_{jk}} \right)^{12} - \left(\frac{\sigma}{r_{jk}} \right)^6 \right], \quad (1)$$

where ϵ_{SL} and σ (0.316 nm) are the energy and length parameters, respectively, and r_{jk} is the distance between two atoms j and k . A cutoff $r_c = 1.3$ nm is applied, as is standard practice in MD. As can be seen from Fig. 1, vapor molecules are so sparse that they have no influence on the droplet. To access the spontaneous spreading regime, droplets are pushed toward the solid as slowly as is computationally feasible (1 m/s), after which the droplet contacts the solid surface and spreads to an equilibrium configuration with contact angle θ_e that depends on ϵ_{SL} .

Further details are in Supplemental Material, Sec. I [41] (within which we also introduce Refs. [42–52]).

First contact.—The shape of the falling droplet can be assumed to be composed of a mean profile (i.e., a circle for quasi-2D and a sphere for 3D droplets) and a fluctuating part that arises from the interfacial thermal fluctuations [53,54]. Consequently, the first contact becomes stochastic, with the axial location being the most probable but a distribution of contact positions (see Supplemental Material, Sec. II [41]) and multiple contacts being also possible. Interestingly, the widths of the distributions are comparable to those for the coalescence of two droplets [54]. However, as will be shown later, while fluctuations of the liquid-vapor interface influence the initial position at contact, they are not dominant during spreading.

Earliest dynamics of wetting.—After a contact is established, the dynamics of wetting are determined by studying the trajectories of groups of molecules near the three-phase zone (TPZ), where all three phases meet. Since the TPZ is not a rigorously defined region, we adopt a sensible classification for liquid molecules to help distinguish the mechanisms of CL motion. Following the scheme detailed in Supplemental Material, Sec. II [41], and referring to Figs. 1(a) and 1(c), the TPZ molecules are colored brown, the interfacial molecules are colored cyan, and the molecules located to the left of the interfacial molecules and above the TPZ molecules are colored purple.

Using our simple tracking algorithm (see Supplemental Material, Sec. II [41]), we clearly identify two regimes of wetting. (A) Rolling regime: Immediately after contact, the attraction from the underlying solid wall causes interfacial (cyan) molecules to collectively traverse the narrow gap between the liquid and the solid advancing the CL laterally in a rolling-type motion [compare Figs. 1(a) and 1(b)]. Notably, in this unconventional wetting mode, the dynamic contact angle is less than 180° . (B) Sliding regime: At a later stage, when the gap width between the interfacial molecules and the solid surface has increased, fewer interfacial molecules are within the influence of the solid wall, and the participation of these molecules in driving the CL reduces. Here, the CL is predominantly driven by the brown- or purple-colored molecules, and it resembles a conventional sliding-type CL motion [compare Figs. 1(c) and 1(d)]. While MD led us to this discovery, to further probe the underlying physics and analyze quantitative data that is difficult to extract from MD (e.g., the velocity field), we develop a macroscopic model of this phenomenon.

A novel continuum model of wetting.—The computational model we discuss and test here is based on the usual Navier-Stokes equations for the droplet, in which interactions with the solid surface are included via the disjoining pressure $p_d(z)$ term in the droplet’s normal stress boundary condition, which is added to the Laplace pressure. For two semi-infinite spaces separated by distance z and filled uniformly by liquid and solid molecules

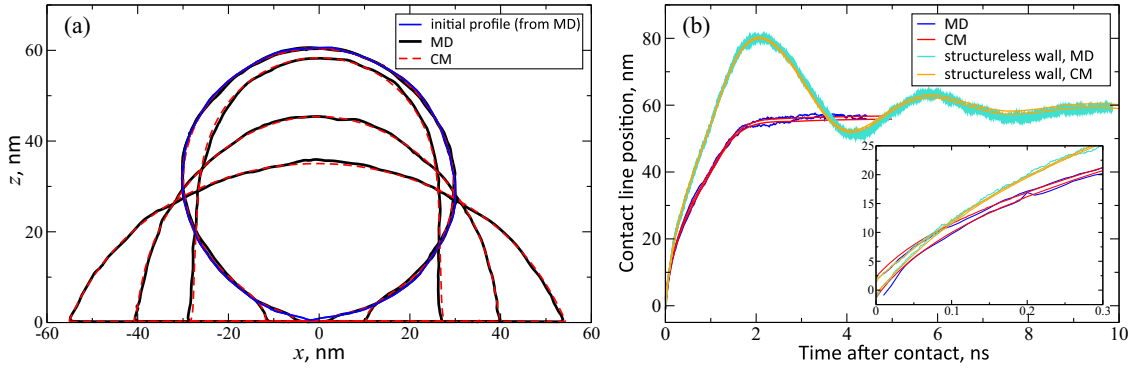


FIG. 2. (a) Droplet profiles from MD ($\epsilon_{SL} = 0.3$ kcal/mol = 2.08×10^{-21} J) and the CM ($A_H = 3.35 \times 10^{-19}$ J and $l_s = 0.9$ nm). The initial shape for the CM (obtained from MD) is colored blue; solid black lines are MD profiles 0.02, 0.1, 0.5, 1, and 2 ns later; dashed red lines are CM profiles at 9 ps later than the MD (see the text). (b) Corresponding CL positions (blue and red lines) compared to (cyan and orange lines) spreading on a structureless wall in MD and perfect slip in the CM ($A_H = 3.5 \times 10^{-19}$ J and $l_s \rightarrow \infty$, shift 7.25 ps), where the reduction in friction leads to an underdamped motion. Simulations have identical initial conditions, so the earliest stages of spreading, shown in the inset in (b), are similar.

(number concentrations n_L and n_S , respectively) interacting via Eq. (1) with energy ϵ_{SL} , we find (see Supplemental Material, Sec. III [41])

$$p_d(z) = -\frac{A_H}{6\pi z^3} \left[1 - \frac{2}{15} \left(\frac{\sigma}{z} \right)^6 \right], \quad (2)$$

where $A_H = 4\pi^2 \epsilon_{SL} n_L n_S \sigma^6$ is the Hamaker constant. We assume Eq. (2) remains valid locally even when the droplet and solid surfaces are not parallel [55,56]. Modeling liquid-solid interactions via the disjoining pressure instead of the body force approach not involving such assumptions is potentially more computationally efficient and produces numerically identical results (see Supplemental Material, Sec. III J [41], for details).

The disjoining pressure (2) turns zero at a finite distance $z_{eq} = (2/15)^{1/6} \sigma \approx 0.226$ nm for our value of σ and approaches $+\infty$ as $z \rightarrow 0$, so that the surface of the droplet will settle at the microscopic distance z_{eq} from the solid surface. No singularities or jumps in any quantities are encountered in this process or after z_{eq} is reached and the droplet starts to spread; in particular, the sharp corner at the CL observed in conventional continuum simulations is replaced by a region of large but finite curvature ($\sim \sigma^{-1}$; see Fig. S9 in Supplemental Material [41]). This approach to avoiding singularities at the CL is distinct from the more common diffuse interface approach [57,58] (as the droplet surface remains sharp) and from precursor film approaches [59]. While assuming no cutoff in the LJ potential is more physical, an expression for the disjoining pressure can also be derived for a finite r_c (Supplemental Material, Sec. III B [41]), and we use it for our comparisons to MD below; all the qualitative considerations above remain valid. At equilibrium, aside from the ‘‘rounded corner,’’ the droplet assumes the expected truncated sphere (circle) shape, with a contact angle

$$\cos \theta_e = -1 + e A_H \gamma^{-1}, \quad (3)$$

where e is an A_H -independent constant, such that $e A_H$ is the interaction energy per unit area obtained by integrating $-p_d$ from z_{eq} to ∞ , and γ is the liquid-vapor surface tension. In our comparisons to MD (here and in Supplemental Material, Sec. III J [41]), we choose A_H to match the observed equilibrium contact line position instead of calculating A_H using its formula; the discrepancy is typically less than a factor of 2 and likely due to the nonuniform liquid density near the solid (see Supplemental Material, Sec. III F [41], for details).

For quantitative agreement with MD, a simple Navier slip model is used on the droplet surface:

$$\tau = \mu l^{-1}(z) u, \quad l^{-1}(z) = l_s^{-1} \exp[-(z - z_{eq})/z_{eq}], \quad (4)$$

where τ is the contribution to the stress component parallel to the solid, u is the velocity component parallel to the solid, μ is the liquid viscosity, and $l(z)$ is the slip length. This interaction kicks in smoothly but rapidly as $z \rightarrow z_{eq}$. The values of slip length in contact, l_s , are obtained from independent MD of Couette flow between parallel plates with the same LJ parameters (see Supplemental Material, Sec. III C [41]).

As an initial condition, the effects of thermal fluctuations can be recreated by starting from a random rather than perfectly spherical or circular droplet shape, either sampled from the canonical ensemble [54] or taken from an MD run to compare to that particular run.

The resulting full set of equations of our continuum model is given in Supplemental Material, Sec. III D [41].

Validation of the continuum model.—The continuum model (CM) is solved using finite elements in COMSOL Multiphysics [60], as detailed in Supplemental Material,

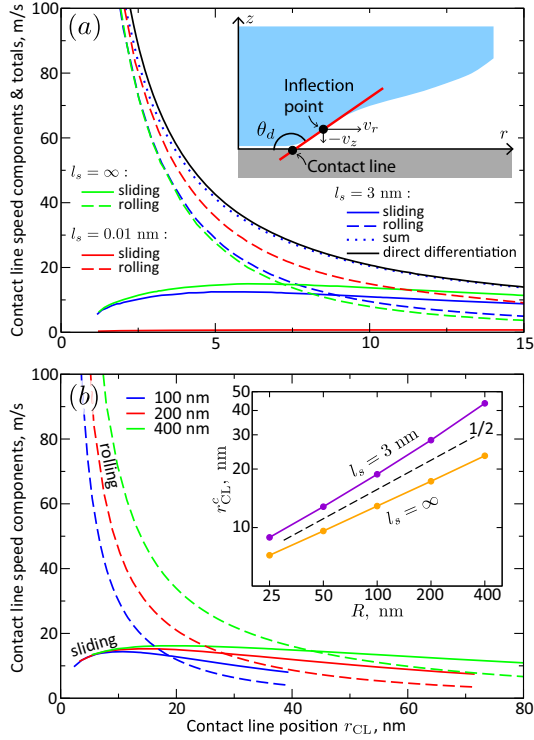


FIG. 3. Sliding and rolling components of the CL speed for a water droplet: (a) with radius $R = 25$ nm, with a moderate ($l_s = 3$ nm), infinite, and extremely small slip length; (b) with radii $R = 100$, 200, and 400 nm and $l_s = 3$ nm. (a) also compares the sum of the sliding and rolling components to the CL speed determined by direct differentiation. All results are obtained from the novel CM simulations.

Sec. III G [41]. We begin by comparing the droplet shapes obtained using the 2D CM to those observed in quasi-2D MD. A profile very close to the initial contact in an MD realization is used as the initial profile for the CM with an initial downward speed of 1 m/s, although the MD droplet will already have acquired a significant velocity at its bottom (see Supplemental Material, Sec. IV A [41]). Despite this approximation, the only visible effect of it is a slight effective “delay” of the spreading process [9 ps in Fig. 2(a); see Supplemental Material, Sec. III J [41]]. There is excellent agreement between the profiles, with the dynamic contact angle changing gradually from 180° to $\theta_e \approx 63^\circ$ (see Supplemental Material, Sec. IV B [41]). Even the asymmetry of the spreading process resulting from an off-center first contact is reproduced well.

Figure 2(b) compares the positions of the CL on both sides obtained with both methods. Again excellent agreement is observed. While there is no sharp CL in either MD or CM, different reasonable definitions give very similar results. For MD, we find the positions of the CL as the x coordinates of the leftmost and rightmost molecules within 0.6 nm of the solid surface, while in the CM they are simply the x coordinates of the intersection points between the droplet profile and the $z = 0.3$ nm line. To isolate the

effects of slip, Fig. 2(b) also presents MD results for a structureless wall, where the solid wall in MD is replaced by a mathematical surface with specular reflection resulting in infinite slip at the interface (see Supplemental Material, Sec. I [41]). Compared to the CM results with perfect slip ($l_s \rightarrow \infty$), excellent agreement is again achieved, with the reduced friction resulting in noticeable inertia-driven oscillations.

Rolling-sliding crossover.—Our CM can now be exploited to study the spreading dynamics of nanodroplets in ways that are challenging for MD. First, we can study 3D spherical droplets where, unlike in MD, axial symmetry can be assumed (although the effect of thermal fluctuations cannot then be studied; this is not our main focus). Second, we can freely adjust the properties of the liquid—they are chosen to match those of water ($\mu = 1$ mPas, $\gamma = 0.07$ N/m, $\rho = 1000$ kg/m³)—and choose $A_H = 10^{-19}$ J (so that $\theta_e \approx 116^\circ$). Third, we study droplets with radii between 25 and as large as 400 nm, which are beyond the reach of MD. Fourth, the cutoff in the LJ potential is eliminated, which is more realistic. Fifth, we are able to vary the slip length independently of other parameters. The length parameter σ is unchanged; the results are only weakly sensitive to its value. Droplets start at the distance 5 or 10 nm from the solid with downward speed of 0.1 m/s; the initial interaction and the effects of nonzero initial speed are negligible.

To study the rolling motion effect more quantitatively, we now identify an inflection point close to the CL typically about 0.5–1 nm above the solid surface. Drawing a tangent line to the droplet’s free surface at this point allows us to define both the CL position, where this line meets the solid, and a dynamic contact angle θ_d ; see the inset in Fig. 3(a). For the CL position, the results match well with the definition (valid also for fluctuating drops and at arbitrarily late times when an inflection point is not unique or cannot be found) based on intersection points between the droplet profile and the $z = 0.3$ nm line, used to plot Fig. 2(b), except when $r_{CL} \lesssim 1$ nm. Data from $r_{CL} \lesssim 1$ nm are eliminated from the plots in Fig. 3. Neglecting the rotation of the tangent line as the droplet spreads, the line translates horizontally and vertically, with the respective speeds v_r and v_z being equal to the corresponding components of the liquid velocity at the inflection point. The CL speed is then

$$v_{CL} = v_r - v_z / \tan(\pi - \theta_d). \quad (5)$$

In Fig. 3(a), we plot the sliding and rolling components of the CL speed as a function of r_{CL} for a droplet of $R = 25$ nm and three different slip lengths: $l_s = \infty$ (perfect slip), $l_s = 3$ nm (close to the MD value), and $l_s = 0.01$ nm (effectively, no slip). The CL speed given by Eq. (5) matches well with that calculated directly by numerically differentiating the corresponding CL position (black solid line). The first term in Eq. (5) corresponds to the droplet

sliding horizontally along the solid, while the second is associated with the vertical bridging motion, as observed in MD (see Fig. S14 [41] for a color map of vertical speeds near the CL). Thus, Eq. (5) decomposes the CL motion into the sliding and rolling components.

For all cases, the rolling speed dominates at early times, in fact, diverging as r_{CL}^{-1} for small r_{CL} , the same as for a spherical droplet impact [$v_{\text{CL}} = 3RV_0/(2r_{\text{CL}})$ [18]]. Measuring $r_{\text{CL}}(t)$, we then find the effective impact speed $V_0 \approx 5.5$ m/s, which is the same in all three cases and considerably exceeds the initial speed of the droplet (0.1 m/s), as the droplet is accelerated by the disjoining pressure prior to contact. Notably, in the no-slip case, the droplet spreads by rolling, and increased rolling speeds are able to partially compensate for a loss of sliding. Larger l_s give increased sliding speeds that are dominant at larger r_{CL} —e.g., for $l_s = 3$ nm, the rolling \rightarrow sliding crossover is at $r_{\text{CL}}^c \approx 9$ nm (about 38% of the equilibrium radius). Notably, in the rolling regime, at a given CL position, the dynamic contact angles θ_d are similar in the three cases and very different from 180° (see Supplemental Material, Sec. IV B [41]), but this does not prevent rolling.

Finally, in Fig. 3(b), we vary the radius of the droplet. In the main plot, the slip length is kept fixed at 3 nm, and while the sliding speed is only weakly dependent on R , the rolling speed increases significantly as the droplet gets larger so that the crossover CL radius r_{CL}^c grows with R . However, as the inset shows, this growth is sublinear (roughly $\propto R^{1/2}$), and, thus, the stage of the spreading dynamics where rolling dominates is less significant as the droplet size increases. For example, for $R = 400$ nm, r_{CL}^c is about 11% of the equilibrium CL radius so that the rolling motion is key for the earliest stages.

Discussion.—The evidence for a $\theta_d < 180^\circ$ rolling-type CL motion driven by disjoining pressure opens up many opportunities, including (i) developing new theories and scaling laws for this regime; (ii) investigating similar mechanisms observed in droplet coalescence [54]; and (iii) using the new continuum model to better design micro- and nanotechnologies that exploit wetting. Furthermore, directions for future analysis (see Supplemental Material, Sec. V [41]) include (a) complete wetting systems, (b) smaller droplets, where the continuum model may fail, (c) more complex slip models, (d) the forming interface process, and (e) heterogeneous surfaces which induce contact line pinning.

The data that support the findings of this study are openly available at [61].

This work was supported by the Engineering and Physical Sciences Research Council (EPSRC) under Grants No. EP/W031426/1, No. EP/S022848/1, No. EP/S029966/1, No. EP/P031684/1, No. EP/R007438/1, No. EP/N016602/1, and No. EP/V012002/1. All MD simulations were run on ARCHER2, the United

Kingdom’s national supercomputing service, funded by an EPSRC/ARCHER2 Pioneer Project. S. P. acknowledges the support from the Leverhulme Trust via the Early Career Fellowship No. ECF-2021-137. The authors also acknowledge the comments and ideas of the referees that enabled us to significantly improve our Letter.

*S.Perumanath@warwick.ac.uk

†ae2173@coventry.ac.uk

‡R.Pillai@ed.ac.uk

§matthew.borg@ed.ac.uk

||j.e.sprittles@warwick.ac.uk

- [1] S. J. Weinstein and K. J. Ruschak, Coating flows, *Annu. Rev. Fluid Mech.* **36**, 29 (2004).
- [2] P. Simpkins and V. Kuck, On air entrainment in coatings, *J. Colloid Interface Sci.* **263**, 562 (2003).
- [3] N. Patra, B. Wang, and P. Král, Nanodroplet activated and guided folding of graphene nanostructures, *Nano Lett.* **9**, 3766 (2009).
- [4] J. C. Fernández-Toledano, B. Braeckeveldt, M. Marengo, and J. De Coninck, How wettability controls nanoprinting, *Phys. Rev. Lett.* **124**, 224503 (2020).
- [5] Y. L. Kong, M. K. Gupta, B. N. Johnson, and M. C. McAlpine, 3D printed bionic nanodevices, *Nano Today* **11**, 330 (2016).
- [6] M. Rauscher and S. Dietrich, Wetting phenomena in nanofluidics, *Annu. Rev. Mater. Res.* **38**, 143 (2008).
- [7] D. Bonn, J. Eggers, J. Indekeu, J. Meunier, and E. Rolley, Wetting and spreading, *Rev. Mod. Phys.* **81**, 739 (2009).
- [8] N. Kavokine, R. R. Netz, and L. Bocquet, Fluids at the nanoscale: From continuum to subcontinuum transport, *Annu. Rev. Fluid Mech.* **53**, 377 (2021).
- [9] L. Xu, W. W. Zhang, and S. R. Nagel, Drop Splashing on a Dry Smooth Surface, *Phys. Rev. Lett.* **94**, 184505 (2005).
- [10] J. M. Kolinski, L. Mahadevan, and S. M. Rubinstein, Drops can bounce from perfectly hydrophilic surfaces, *Europhys. Lett.* **108**, 24001 (2014).
- [11] J. Qian and H. Gao, Scaling effects of wet adhesion in biological attachment systems, *Acta Biomater.* **2**, 51 (2006).
- [12] M. J. Vogel and P. H. Steen, Capillarity-based switchable adhesion, *Proc. Natl. Acad. Sci. U.S.A.* **107**, 3377 (2010).
- [13] J. C. Bird, S. Mandre, and H. A. Stone, Short-Time Dynamics of Partial Wetting, *Phys. Rev. Lett.* **100**, 234501 (2008).
- [14] A. Eddi, K. G. Winkels, and J. H. Snoeijer, Short time dynamics of viscous drop spreading, *Phys. Fluids* **25**, 013102 (2013).
- [15] K. G. Winkels, J. H. Weijs, A. Eddi, and J. H. Snoeijer, Initial spreading of low-viscosity drops on partially wetting surfaces, *Phys. Rev. E* **85**, 055301(R) (2012).
- [16] A.-L. Biance, C. Clanet, and D. Quéré, First steps in the spreading of a liquid droplet, *Phys. Rev. E* **69**, 016301 (2004).
- [17] Y. D. Shikhmurzaev, Reflections on reflections of Dieter Bothe on the ‘litmus test’ for mathematical models of dynamic wetting, *Eur. Phys. J. Spec. Top.* **229**, 1989 (2020).

- [18] J. Philippi, P.-Y. Lagr e, and A. Antkowiak, Drop impact on a solid surface: Short-time self-similarity, *J. Fluid Mech.* **795**, 96 (2016).
- [19] C. Huh and L. Scriven, Hydrodynamic model of steady movement of a solid/liquid/fluid contact line, *J. Colloid Interface Sci.* **35**, 85 (1971).
- [20] E. B. Dussan, On the spreading of liquids on solid surfaces: Static and dynamic contact lines, *Annu. Rev. Fluid Mech.* **11**, 371 (1979).
- [21] P. G. de Gennes, Wetting: Statics and dynamics, *Rev. Mod. Phys.* **57**, 827 (1985).
- [22] Y. D. Shikhmurzaev, *Capillary Flows with Forming Interfaces* (Chapman and Hall/CRC, London, 2007).
- [23] E. B. Dussan V., The moving contact line: The slip boundary condition, *J. Fluid Mech.* **77**, 665 (1976).
- [24] L. M. Hocking, A moving fluid interface on a rough surface, *J. Fluid Mech.* **76**, 801 (1976).
- [25] Y. D. Shikhmurzaev, Moving contact lines in liquid/liquid/solid systems, *J. Fluid Mech.* **334**, 211 (1997).
- [26] C. G. Ngan and E. B. Dussan V., The moving contact line with a 180° advancing contact angle, *Phys. Fluids* **27**, 2785 (1984).
- [27] L. Mahadevan and Y. Pomeau, Rolling droplets, *Phys. Fluids* **11**, 2449 (1999).
- [28] E. S. Benilov and M. Vynnycky, Contact lines with a 180° contact angle, *J. Fluid Mech.* **718**, 481 (2013).
- [29] O. Schnitzer, A. M. J. Davis, and E. Yariv, Rolling of non-wetting droplets down a gently inclined plane, *J. Fluid Mech.* **903**, A25 (2020).
- [30] T. Blake and J. Haynes, Kinetics of liquid-liquid displacement, *J. Colloid Interface Sci.* **30**, 421 (1969).
- [31] T. D. Blake, The physics of moving wetting lines, *J. Colloid Interface Sci.* **299**, 1 (2006).
- [32] R. G. Cox, The dynamics of the spreading of liquids on a solid surface. Part 1. Viscous flow, *J. Fluid Mech.* **168**, 169 (1986).
- [33] O. V. Voinov, Hydrodynamics of wetting, *Fluid Dyn.* **11**, 714 (1977).
- [34] J. H. Snoeijer and B. Andreotti, Moving contact lines: Scales, regimes, and dynamical transitions, *Annu. Rev. Fluid Mech.* **45**, 269 (2013).
- [35] D. Richard and D. Qu er e, Viscous drops rolling on a tilted non-wettable solid, *Europhys. Lett.* **48**, 286 (1999).
- [36] M. P. Allen and D. J. Tildesley, *Computer Simulation of Liquids*, 2nd ed. (Oxford University Press, New York, 2017).
- [37] J. Koplik and J. R. Banavar, Continuum deductions from molecular hydrodynamics, *Annu. Rev. Fluid Mech.* **27**, 257 (1995).
- [38] J. De Coninck and T. D. Blake, Wetting and molecular dynamics simulations of simple liquids, *Annu. Rev. Mater. Res.* **38**, 1 (2008).
- [39] Y. Nakamura, A. Carlson, G. Amberg, and J. Shiomi, Dynamic wetting at the nanoscale, *Phys. Rev. E* **88**, 033010 (2013).
- [40] V. Molinero and E. B. Moore, Water modeled as an intermediate element between carbon and silicon, *J. Phys. Chem. B* **113**, 4008 (2009).
- [41] See Supplemental Material at <http://link.aps.org/supplemental/10.1103/PhysRevLett.131.164001> which contains technical details that are complementary to this Letter. We discuss (I) the molecular dynamics simulation details, (II) the first contact and the following rolling regime in wetting, (III) the details of the novel continuum model for wetting, (IV) additional results from the new continuum model, and (V) some further exploration of the rolling mode using the continuum model. Readers are also invited to view the supplemental movie.
- [42] J. L. Abascal and C. Vega, A general purpose model for the condensed phases of water: TIP4P/2005., *J. Chem. Phys.* **123**, 234505 (2005).
- [43] L. Bocquet and J.-L. Barrat, Hydrodynamic boundary conditions, correlation functions, and Kubo relations for confined fluids, *Phys. Rev. E* **49**, 3079 (1994).
- [44] Y. Zhang, J. E. Sprittles, and D. A. Lockerby, Nanoscale thin-film flows with thermal fluctuations and slip, *Phys. Rev. E* **102**, 053105 (2020).
- [45] G. J. Wang and N. G. Hadjiconstantinou, Universal molecular-kinetic scaling relation for slip of a simple fluid at a solid boundary, *Phys. Rev. Fluids* **4**, 064201 (2019).
- [46] N. G. Hadjiconstantinou and M. M. Swisher, On the equivalence of nonequilibrium and equilibrium measurements of slip in molecular dynamics simulations, *Phys. Rev. Fluids* **7**, 114203 (2022).
- [47] T. Young, III: An essay on the cohesion of fluids, *Phil. Trans. R. Soc. London* **95**, 65 (1805).
- [48] M. V. Chubynsky, K. I. Belousov, D. A. Lockerby, and J. E. Sprittles, Bouncing Off the Walls: The Influence of Gas-Kinetic and van der Waals Effects in Drop Impact, *Phys. Rev. Lett.* **124**, 084501 (2020).
- [49] I. Chakraborty, M. V. Chubynsky, and J. E. Sprittles, Computational modelling of Leidenfrost drops, *J. Fluid Mech.* **936** (2022).
- [50] R. A. Cairncross, P. R. Schunk, T. A. Baer, R. R. Rao, and P. A. Sackinger, A finite element method for free surface flows of incompressible fluids in three dimensions. Part I. Boundary fitted mesh motion, *Int. J. Numer. Methods Fluids* **33**, 375 (2000).
- [51] Y. D. Shikhmurzaev, Moving contact lines and dynamic contact angles: A ‘litmus test’ for mathematical models, accomplishments and new challenges, *Eur. Phys. J. Spec. Top.* **229**, 1945 (2020).
- [52] J. Zhang, P. Wang, M. K. Borg, J. M. Reese, and D. Wen, A critical assessment of the line tension determined by the modified Young’s equation, *Phys. Fluids* **30**, 082003 (2018).
- [53] D. G. A. L. Aarts, M. Schmidt, and H. N. W. Lekkerkerker, Direct visual observation of thermal capillary waves, *Science* **304**, 847 (2004).
- [54] S. Perumanath, M. K. Borg, M. V. Chubynsky, J. E. Sprittles, and J. M. Reese, Droplet Coalescence is Initiated by Thermal Motion, *Phys. Rev. Lett.* **122**, 104501 (2019).
- [55] A. Oron, S. H. Davis, and S. G. Bankoff, Long-scale evolution of thin liquid films, *Rev. Mod. Phys.* **69**, 931 (1997).
- [56] R. V. Craster and O. K. Matar, Dynamics and stability of thin liquid films, *Rev. Mod. Phys.* **81**, 1131 (2009).
- [57] Y. Sui, H. Ding, and P. D. Spelt, Numerical simulations of flows with moving contact lines, *Annu. Rev. Fluid Mech.* **46**, 97 (2014).

- [58] P. Seppacher, Moving contact lines in the Cahn-Hilliard theory, *Int. J. Eng. Sci.* **34**, 977 (1996).
- [59] J. A. Diez and L. Kondic, Computing three-dimensional thin film flows including contact lines, *J. Comput. Phys.* **183**, 274 (2002).
- [60] COMSOL Ltd., Cambridge, United Kingdom.
- [61] M. Chubynsky, S. Perumanath, R. Pillai, J. Sprittles, and M. Borg, Rolling and Sliding modes of Droplet Spreading: Molecular Simulations and a Continuum Approach (2023), [10.7488/ds/7516](https://doi.org/10.7488/ds/7516).